

# Searching for Mass Concentrations with Precision Pulsar Timing

John M. LoSecco<sup>1\*</sup>

<sup>1</sup>*Physics and Astronomy Department, University of Notre Dame, Notre Dame, IN 46556-5670, USA*

Accepted XXX. Received YYY; in original form ZZZ

## ABSTRACT

This paper searches for evidence of mass concentrations along the path of radio pulses in the IPTA survey data release. Radio pulse travel times are influenced via gravitational fields along the path from the source to the observer. Transient time delays in transit are a useful measure of the matter distribution along the path. Many pulsars have very well understood timing solutions with predictable arrival times and can be used to sample the mass variation. Changes in the source, observer and mass concentration positions produce changes in arrival times which can be significant for precision pulsar times. Nine candidates are reported from this search. After red noise reduction the number of candidates drops to two. When the epoch at the encounter times are removed the candidates vanish. Delayed and early event candidates are found at about the same rate. There is no clear evidence for a signal of gravitational delays from this search.

**Key words:** dark matter pulsars: general proper motions time gravitation

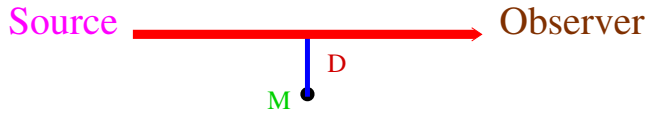


**Figure 1.** An illustration of the source to observer geometry. The impact parameter  $D$  and the gravitating mass  $\mathcal{M}$  are shown.

## 1 INTRODUCTION

Gravitational interactions have been suggested as a source of transient distortions in pulsar arrival time. [Larchenkova \(1995\)](#). Recently efforts have been made to understand and correct for a broad class of timing distortions in pulsar arrival times with results approaching microsecond resolution. This suggests that searching these data may help strengthen models of galactic mass distributions.

In this note we search for the relativistic delay in pulsar pulses due to encounters with the gravitational fields of masses distributed close the path of source to observer, as illustrated in figure 1. A static mass distribution would add an unmeasurable constant time delay to the signal, so just as in other mass concentration searches [Wyrzykowski \(2022\)](#) one looks for a time delay caused by a transient encounter.

The accumulated time delay is given by [Shapiro \(1964\)](#); [Larchenkova \(2007\)](#):

$$\Delta T = -\frac{2G\mathcal{M}}{c^3} \ln(1 - \hat{R} \cdot \hat{s}) \quad (1)$$

where  $\frac{2G\mathcal{M}}{c^3}$  is the Schwarzschild radius divided by the speed

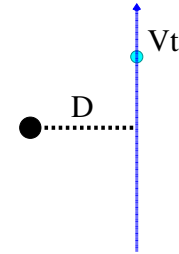


**Figure 2.** The time dependent geometry of the pulsar - mass concentration cosine as viewed by the observer. The Z axis goes from the observer to the pulsar (dot on the left). The point of closest approach is a distance  $D$  along the X axis. The Y coordinate is upward along the projected speed of the mass concentration. The displacement along Y is taken as  $Vt$ . The mass concentration is in the plane at  $(D, Vt)$ .

of light and  $\hat{R} \cdot \hat{s}$  is the cosine of the angle, as viewed from the observer, between the source of the pulse and the source of the gravitational field created by mass  $\mathcal{M}$ .

Pulsar timing arrays [Kerr \(2021\)](#) have improved arrival time fits for pulses and modeled the various known sources of time deviations in the transit time. Orbital motion of the source and the observer can be fit and removed. Observing at multiple frequencies permits removal of frequency dependent plasma delays. Even the relativistic delay caused by a massive companion of the pulsar can be fit and removed.

\* E-mail: losecco@nd.edu

## 2 GRAVITATIONAL TIME DELAY

In this paper we fit the pulsar timing residuals of the IPTA survey sources [IPTA \(2019\)](#) to a 4 parameter model of an encounter of the beam with a mass source moving with constant speed in the plane of the observation.

[Larchenkova \(1995\)](#) suggest the 4 parameter fit of equation 2.

$$\Delta T = -M \ln \left( 1 - \frac{1}{\sqrt{1 + (v(t - t_0))^2 + d^2}} \right) \quad (2)$$

with  $M = \frac{2GM}{c^3}$  as the mass of the source of the field (in units of microseconds),  $t_0$  is the time of the closest encounter,  $v$  is the (assumed) constant projected speed of the encounter and  $d$  is the distance of closest approach, at  $t = t_0$ . For reference  $M_{sun}$  is 9.85 microseconds. To be more precise  $d$  is the tangent of the angle of closest approach and  $v(t - t_0)$  is the tangent of the angle from the point of closest approach to the location at time  $t$ .

Equation 2 is found by explicitly calculating the value of  $\hat{R} \cdot \hat{s}$  in the geometry shown in figure 2. Take the  $\hat{z}$  axis along the direction from the observer to the pulsar. The distance from the pulsar beam path to the mass concentration candidate point of closest approach is  $D$ . The direction from the pulsar beam path to the mass concentration candidate point of closest approach defines the  $\hat{x}$  axis. The vertical axis in the figure is the  $\hat{y}$  axis and is the direction of motion of the mass concentration candidate. The  $Z$  distance is arbitrary but we can take it as the distance along the  $\hat{z}$  axis to the point of closest approach of the beam to the mass concentration candidate. Figure 2 is drawn in the plane perpendicular to the  $\hat{z}$  axis at distance  $Z$ . In this coordinate system  $\vec{R} = (0, 0, Z)$  and  $\vec{s} = (D, Vt, Z)$ .

$$\begin{aligned} \hat{R} \cdot \hat{s} &= \frac{Z^2}{Z \times \sqrt{Z^2 + (Vt)^2 + D^2}} \\ &= \frac{Z^2}{Z^2 \sqrt{1 + (vt)^2 + d^2}} \\ &= \frac{1}{\sqrt{1 + (vt)^2 + d^2}} \end{aligned} \quad (3)$$

which is equation 2 with  $d = D/Z$  and  $v = V/Z$ .

Equation 3 has some physical consequences.  $d$  is the tangent of an angle and  $v$  is the time derivative of the tangent of an angle. If the physical relative velocity  $V$  between the pulsar and the moving matter is roughly constant more distant encounters will have slower time delay encounters.  $d$  also decreases with greater distance which means that the maximum amplification at closest approach will be larger for distant objects. This is essentially parallax. Due to the smaller  $v$  distant encounters may not return to baseline over the search window. One may get overlapping encounters which will change the shape of the observed delay.

## 3 THE DATA

The IPTA release [IPTA \(2019\)](#) includes 65 millisecond pulsars and their fits. The Version B TCB data was processed with *Tempo2* [Edwards \(2006\)](#), with and without maximum-likelihood red noise subtraction, to provide residuals, the deviation of the pulse arrival time from the time estimated by

the model. These residuals hold information about potential encounters with massive bodies on route to the detector.

The IPTA data release 2 combines data from prior releases, EPTA 1, NANOGrav 9-year, PPTA and their extensions. The observations have been made by seven different radio telescopes (Effelsberg, Lovell, Nançay, Westerbork, Green Bank, Arecibo, Parkes) The pulsar data samples span varying time intervals from 231 to 10753 days and have from 116 to 17487 fitted pulses. A total of 210148 pulse residuals over a total time period of 255327 MJD are provided in the release.

## 4 METHOD

The method used has two parts. The first part searches for signal delay candidates over a limited portion of the recorded data. Once found a local fit is done on that candidate to recover the fit parameters.

Based on gravitational lensing results the encounters are expected to occur over a period of weeks or months. The data sample span periods from less than a year to almost 30 years. Reliable fits also require many more data points to be fit compared to the four parameters to be measured. The method adopted is to fit overlapping regions of at about 120 consecutive residuals, less if there is not enough data to provide 120 samples. The initial fit is done with simulated annealing which searches the four dimensional parameter space. This is followed by a Levenberg-Marquardt nonlinear fitter. A modest event candidate is refit with the candidate time at the center of the interval. When possible the time width of the fit is chosen to be the point where the peak has dropped to 10% of its maximum height. The peak position and width are based on the parameters extracted from the search step. The fit is sensitive to the tails of the fit function so having two tails to fit helps reject noise. If the candidate time is near either end of the data sample that tail is truncated. Using a sample size large compared to the encounter time makes the fit more sensitive to fluctuations in the underlying tempo2 fit since the fit curve returns to zero on both sides of an encounter. To proceed from the search fit to the centered fit the search result must have a log likelihood ratio test at the 95% level. The fit itself should have an Anderson-Darling test for gaussian residuals at the 95% level and the absolute value of the fitted mass,  $|M|$  must be at least 2 time its  $\sigma$ . Accepting  $M < -2\sigma$  is included to study potential background fluctuations indicated by negative time delays with the same time structure expected from a point mass.

The selection is tightened to  $3\sigma$  plus the requirement that  $\chi^2/DOF$  probability is greater than 10% is applied to the centered fit before it can be accepted as a Shapiro delay candidate.

## 5 TECHNICAL DETAILS

From equation 1 it is clear that the fit can diverge as  $\hat{R} \cdot \hat{s} \rightarrow 1$ . Since the residual data is finite it is unlikely that the solution will fall on this point but the fitter may still explore this region to approach the best fit. Due to finite precision of computer representations of numbers  $1 - \cos \theta$  may approach 0 more rapidly due to loss of precision. The fitter uses the “log1p” function of  $-\cos \theta$  to delay the round

**Table 1.** There are 9 candidates after duplicates have been removed. Nine pulsars are represented. The first 4 columns give details of the fit sample including the time duration of the sample and the number of points fit. The fifth column gives the RMS value of the residuals used in the fit as a measure of the noise level in the sample. The last 4 columns give the result of the centered 10% fit including the  $\chi^2$  confidence of the fit, the mass fitted, the significance of the mass fit in  $\sigma$ 's and the maximum amplitude of the fit. The RMS and the maximum amplitude are given in microseconds. The masses are given in solar masses

Pulsar	Sample	Duration	Count	RMS	Significance	$\mathcal{M} \pm \sigma_{\mathcal{M}}$ in $\mathcal{M}_{Sun}$	$\mathcal{M}/\sigma_{\mathcal{M}}$	MaxAmp
J1744-1134	94	57.8	441	2.481	0.9986	$0.002497 \pm 0.0006352$	3.93	1.03
J0613-0200	23	239.4	421	4.752	0.9982	$0.01244 \pm 0.003663$	3.396	4.471
J1600-3053	105	122.7	378	1.555	0.9153	$-0.005644 \pm 0.001714$	-3.292	-1.645
J1939+2134	226	70.8	347	45.71	0.8367	$-0.3258 \pm 0.03308$	-9.848	-50.39
J2145-0750	127	90.9	447	11.48	0.7004	$-0.02353 \pm 0.005579$	-4.218	-14.49
J1747-4036	25	80.8	492	6.215	0.2668	$0.0335 \pm 0.005774$	5.803	10.84
J1955+2908	17	109.8	386	3.843	0.2096	$0.01039 \pm 0.002965$	3.503	4.319
J1643-1224	3	226.7	107	6.98	0.2025	$0.04918 \pm 0.00765$	6.428	9.98
J1824-2452	1	554.5	103	1.985	0.1607	$-0.05956 \pm 0.01748$	-3.406	-3.237

off error in the logarithm function evaluation. At even smaller values of  $\theta$  the approximation of  $1 - \cos \theta = \theta^2/2$  is used as the argument to the logarithm. Eventually that is replaced with  $\ln(\theta^2/2) = 2\ln(\theta) - \ln(2)$ . This provides access to a maximum amplification of about 1490 with standard double precision calculations.

The transition from search to fit uses the preliminary fitted velocity from the search to determine the temporal range of the fit. Ideally one wants a time range in which the fit is dominated by the signal and not the asymptotic tails which should go to zero. The first attempt is to construct a time symmetric region about the candidate time with the amplitude dropping to 10% of the peak height. In the case of a very local fluctuation the search fitted velocity is very large and one ends up with very few timing residuals in the narrow time range. To get more statistics the refit region is expanded to get at least 100 points.

Alternatively a systematic shift in the residuals raises the baseline. There is no baseline parameter in the fit so this is turned into a very small velocity. The small velocity results in a very large time range for the refit, sometimes including the whole data sample for the pulsar. The refitting for nearby search regions then have a large overlap, reducing their independence. In this case the refit is shortened to under 500 residuals.

In both cases the refit sample is centered on the candidate to the extent possible and the initial values for the refit parameters are those taken from the search. “to the extent possible” is needed since the data itself is not uniformly sampled in time and is a merger of data from multiple instruments. The search time is put in the middle of the refit sample. Gaps in the data sample and different sampling rates may cause the centered fit to not have the same number of residuals before and after the event time. Lower or upper time limits of the whole data sample also restrict the range for the centered fit.

In the case of low velocities this adjustment procedure may produce a small bias against a true signal with the direction of proper motion close to the line of sight. On the other hand the search samples may have a non-zero offset, perhaps coming from very long period signals. A symptom of such an offset is a very small value for  $v$ . If  $v\Delta t < 10$  mrad the offset is removed by subtracting the sample mean from the sample.  $\Delta t$  is the actual time length of the fit sample. This baseline adjustment was not needed for any of the candidate encounters in this paper.

An MCMC based search was used to explore the parameter

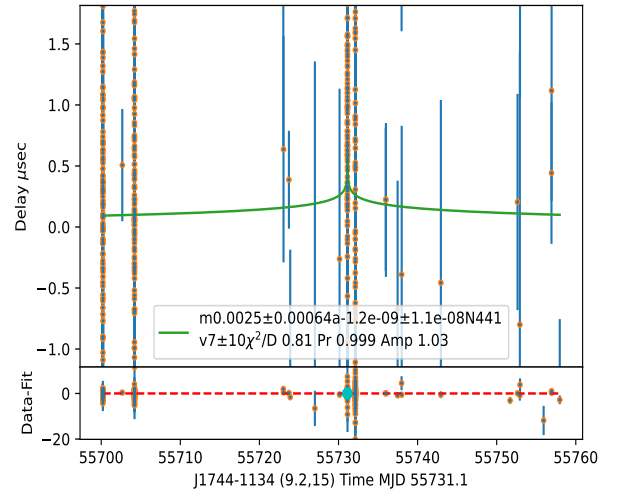


**Figure 3.** The fit for J1744-1134 in the DM subtracted sample

space near the solution to improve the error estimates. A fit was accepted as a candidate if  $\mathcal{M}/\sigma_{\mathcal{M}} > 3$  and the  $\chi^2/DOF$  probability exceed 0.1.

## 6 RESULTS

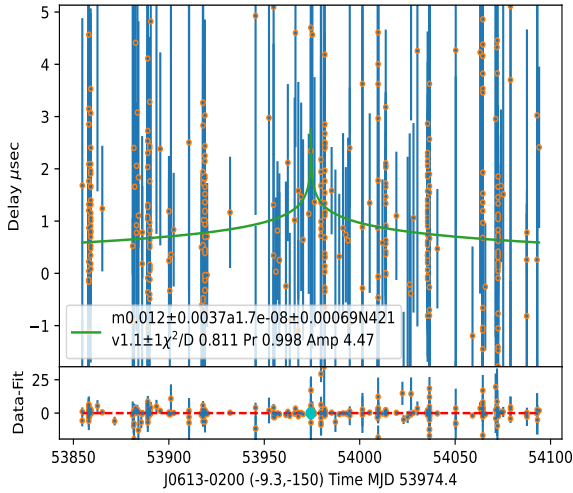
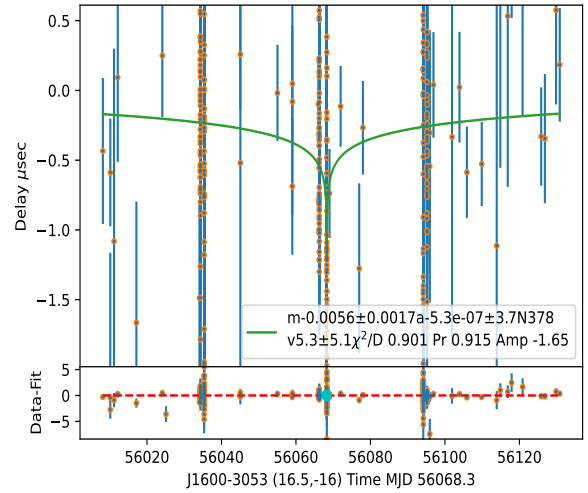
The initial search was done on data with dispersion measure (DM) corrections but not red noise subtraction. 1833 candidates pass the search criteria to be recentered and refit. After the refit 10 of these have  $|\mathcal{M}/\sigma_{\mathcal{M}}| > 3$ . (37 of these have  $|\mathcal{M}/\sigma_{\mathcal{M}}| > 2$ ). All 10 of these have a fit with a  $\chi^2/DOF$  probability  $> 0.1$ , the criteria in the centered fit to become a final event candidate. The results of this search are shown in table 2. Since the search uses overlapping regions and the centered fit can extend the fit into regions already fit there are duplicate candidates in some cases. Since the data samples do not overlap completely the duplicates are not identical but the date is very close and the other parameters agree to fractions of a  $\sigma$ . One duplicate (J1747-4036) has been removed from the table. Table 1 lists the results of the search. The table includes details about the sample and results of the fit

**Table 2.** Summary of the fit parameters for the 9 events

Pulsar	Sample	$\mathcal{M} \pm \sigma_{\mathcal{M}}$	$d \pm \sigma_d$	$v \pm \sigma_v$	$T_0 \pm \sigma_{T_0}$
J1744-1134	94	$0.002497 \pm 0.0006352$	$-0.00000006618 \pm 0.0000006069$	$7.024 \pm 10.37$	$55731 \pm 0.000025036$
J0613-0200	23	$0.01244 \pm 0.003663$	$0.0000009747 \pm 0.03935$	$1.071 \pm 1.031$	$53974 \pm 0.6218$
J1600-3053	105	$-0.005644 \pm 0.001714$	$-0.00003053 \pm 213.8$	$5.283 \pm 5.063$	$56068 \pm 1.3192$
J1939+2134	226	$-0.3258 \pm 0.03308$	$0.0316 \pm 0.024$	$0.02235 \pm 0.01407$	$56630 \pm 3.7714$
J2145-0750	127	$-0.02353 \pm 0.005579$	$2.171\text{E-}12 \pm 0.0000001042$	$-0.000006982 \pm 0.00002607$	$56487 \pm 2.0464$
J1747-4036	25	$0.0335 \pm 0.005774$	$0.000006053 \pm 0.0000518$	$833 \pm 1545$	$56354 \pm 0.0000010407$
J1955+2908	17	$0.01039 \pm 0.002965$	$-0.00000005551 \pm 0.0000005509$	$0.4187 \pm 0.7247$	$56426 \pm 0.000045784$
J1643-1224	3	$0.04918 \pm 0.00765$	$0.002731 \pm 0.005094$	$1.669 \pm 1.257$	$53292 \pm 0.082416$
J1824-2452	1	$-0.05956 \pm 0.01748$	$5.143 \pm 0.1742$	$4.426 \pm 1.654$	$53841 \pm 5.7474$

**Table 3.** Summary of the data sample of the 9 pulsars

Pulsar	Sample Length (MJD)	Sample Size	Mean Residual
J1744-1134	7262.00	9834	9.39E-18
J0613-0200	5863.88	9322	-1.22E-17
J1600-3053	4493.04	9006	6.31E-18
J1939+2134	10753.43	13659	3.20E-15
J2145-0750	7243.47	8456	1.08E-16
J1747-4036	609.33	2771	-8.21E-17
J1955+2908	2967.89	1459	0.00380
J1643-1224	7356.24	8136	-5.59E-17
J1824-2452	2063.30	276	0

**Figure 4.** The fit for J0613-0200 in the DM subtracted sample**Figure 5.** The fit for J1600-3053 in the DM subtracted sample

including the fitted mass and the  $\chi^2/DoF$  probability. The number of residuals fit, the duration of the sample (in MJD) and the RMS of the sample and the maximum amplitude of the fit, in microseconds, are also listed

Table 2 includes the full list of the fitted parameters including  $d$ ,  $v$  and the time of closest approach  $t_0$ . Note that there is not necessarily a data point taken at closest approach. There are no selection constraints on the values or significance of these other parameters. These data are also printed on the plots.

## 7 FIGURES

Figures showing all the fits are displayed in Figures 3 to 11. The figures are ordered from high to low by  $\chi^2/DOF$  probability. Each figure has an upper panel showing the data and the fitted curve. The lower panel shows the data minus the fitted value of the delay curve, the new residuals. The dashed line on the lower panel is zero and the large point marks the position of the peak in the upper plot. The vertical axes on each plot are individually scaled and range from microseconds to tens of microseconds. Values for “vel”= $v$  and “ang”= $a$  printed on the plots are scaled by 10,000 to reduce the number of zeros to the right of the decimal. The plot legend also includes the number of points fit (N), the  $\chi^2/DOF$ , the  $\chi^2$

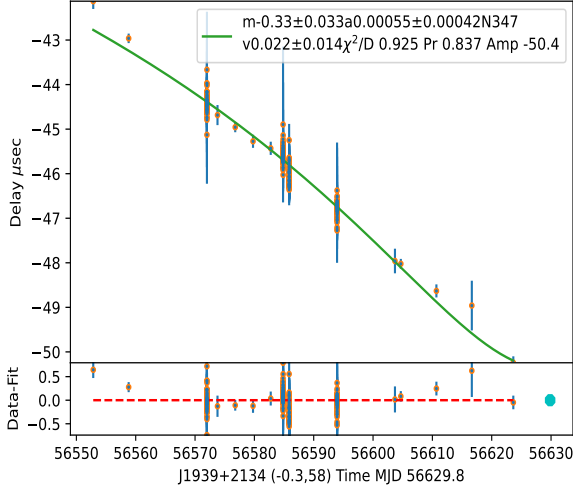


**Figure 6.** The fit for J1939+2134 in the DM subtracted sample

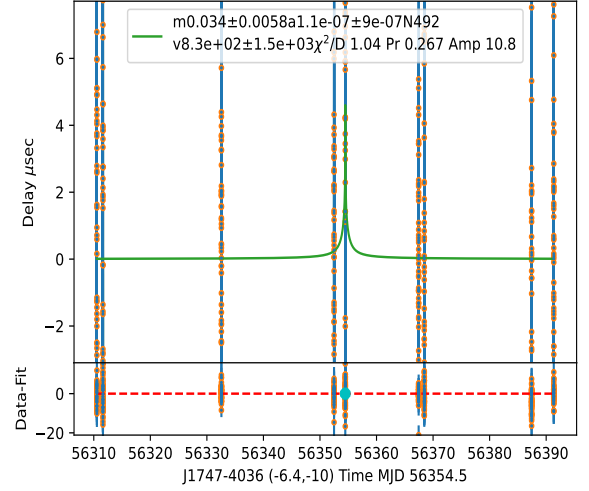


**Figure 8.** The fit for J1747-4036 in the DM subtracted sample

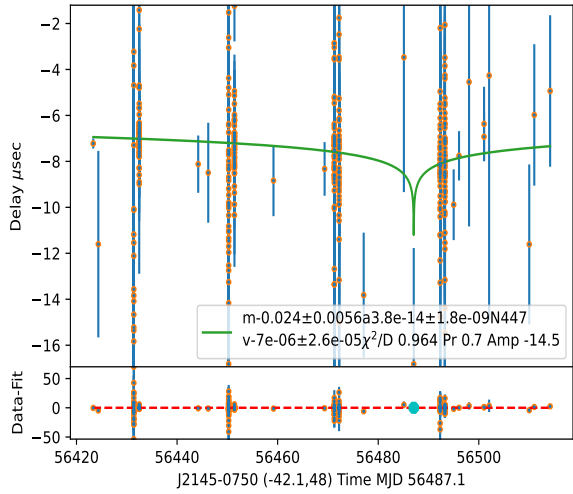


**Figure 7.** The fit for J2145-0750 in the DM subtracted sample

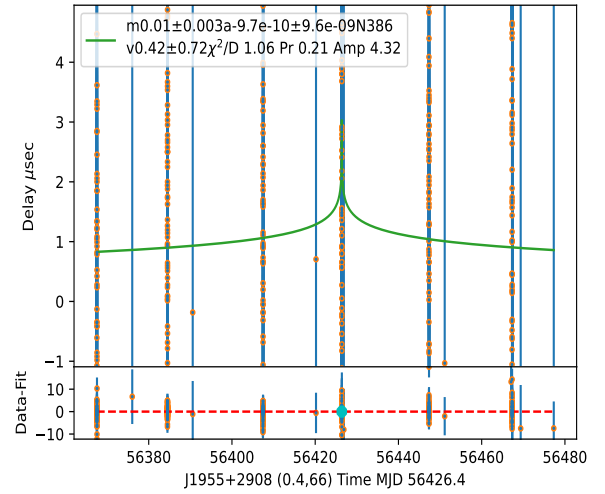


**Figure 9.** The fit for J1955+2908 in the DM subtracted sample

probability and the maximum amplitude of the fitted curve (Amp).

## 8 TIMING NOISE

There are known sources of timing noise (also known as red noise) that can mimic a Shapiro delay signature (Goncharov (2021)). The search for gravitational encounters has been conducted on the same data sample with additional processing to remove timing (red) noise. Two candidates remain. Figure 12 has the plots for these events. Tables 4, 5 and 6 have the details.

Pulsar J2043+1711 has a candidate encounter in the red noise subtracted data but the event didn't make the cut in

the dispersion measure sample search. The event was found in the initial dispersion measure sample at the same location, with the same mass and velocity and the same  $\chi^2/DOF$ . It did not make the cut to proceed to a 10% symmetric fit because the mass found was only 1.7 times  $\sigma_M$ . The searched samples overlap so even when missed in sample 13 it could have been seen in the previous sample. J2043+1711 sample 12 also failed to move to the 10% centered fit by failing the  $M/\sigma_M > 2$  cut.

## 9 DISCUSSION

This search has failed to find definitive evidence for a significant occurrence of gravitational induced delays as modeled in

**Table 4.** There are 2 candidates after duplicates have been removed. Two pulsars are represented. The columns are the same as in Table 1

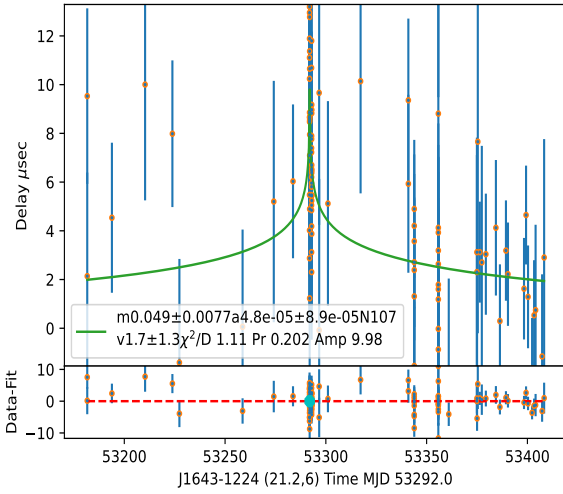
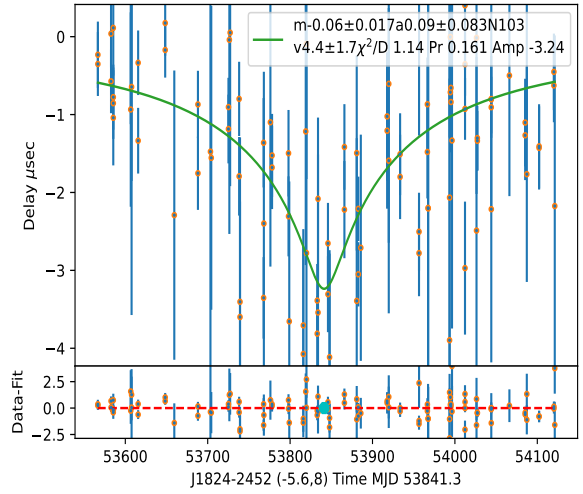
Pulsar	Sample	Duration	Count	RMS	Significance	$\mathcal{M} \pm \sigma_{\mathcal{M}}$ in $\mathcal{M}_{Sun}$	$\mathcal{M}/\sigma_{\mathcal{M}}$	MaxAmp
J1747-4036	25	80.8	492	6.215	0.2691	$0.03391 \pm 0.00559$	6.065	11.43
J2043+1711	13	100.7	483	1.408	0.2329	$-0.002218 \pm 0.000565$	-3.925	-1.155

**Table 5.** Summary of the fit parameters for the 2 events. The columns are the same as in Table 2

Pulsar	Sample	$\mathcal{M} \pm \sigma_{\mathcal{M}}$	$d \pm \sigma_d$	$v \pm \sigma_v$	$T_0 \pm \sigma_{T_0}$
J1747-4036	25	$0.03391 \pm 0.00559$	$0.000003011 \pm 0.00003463$	$819.9 \pm 1478$	$56354 \pm 0.00000067269$
J2043+1711	13	$-0.002218 \pm 0.000565$	$2.688\text{E-}10 \pm 0.000002152$	$168.7 \pm 285.1$	$56298 \pm 0.00000037965$

**Table 6.** Summary of the data sample of the 2 pulsars. The columns are the same as in Table 3

Pulsar	Sample Length (MJD)	Sample Size	Mean Residual
J1747-4036	609.33	2771	-8.21E-17
J2043+1711	833.75	1382	5.14e-18

**Figure 10.** The fit for J1643-1224 in the DM subtracted sample**Figure 11.** The fit for J1824-2452 in the DM subtracted sample

this search in the 65 pulsar IPTA2 data sample. Four out of nine of the events in Table 1 and one out of two of the events in the red noise subtracted table 6 have  $\mathcal{M} < 0$  which is unexpected from a lump of matter. The fact that the number of positive and negative events are similar suggests a common source.

The red noise subtracted candidates have small masses and high velocities which could be due to an unmodeled short period detector time shift. The referee suggested removing the epoch at the fitted time and refitting. This removes the candidate encounters, verifying the hypothesis. True signals should span many epochs, if only to reduce susceptibility to noise.

The relativistic time delay due to masses in the source system or in the solar system are found and removed. Why is the common local distribution of matter not manifest in the data sample, even if most of the gravitational potential, such as that due to dark matter is smooth?

Equation 2 has a time dependence on  $v$ . As seen after equation 3  $v$  is a time rate of change of the angular separation

between the pulsar and the matter concentration of the encounter,  $v = V/Z$ . As such, it decreases with distance. The search has been conducted for encounters that return to a baseline of 10% of the peak. If  $v$  is small the delay may not return to a baseline value during the duration of the sample. The absence of a change in the delay time on the scale of the observations make a gravitational induced delay indistinguishable from other sources of time delays.

Extending the search to lower  $v$  is possible. Most of the pulsars have many years of data. But increasing the residual sample length introduces the possibility of overlapping signals which may not fit this simple model.

## 10 CONCLUSIONS

This article presents a search for massive objects via their gravitational fields. A four parameter fit has failed to identify convincing sources. In principle the parameters in the fits were unbounded. In practice the nature of the data sample

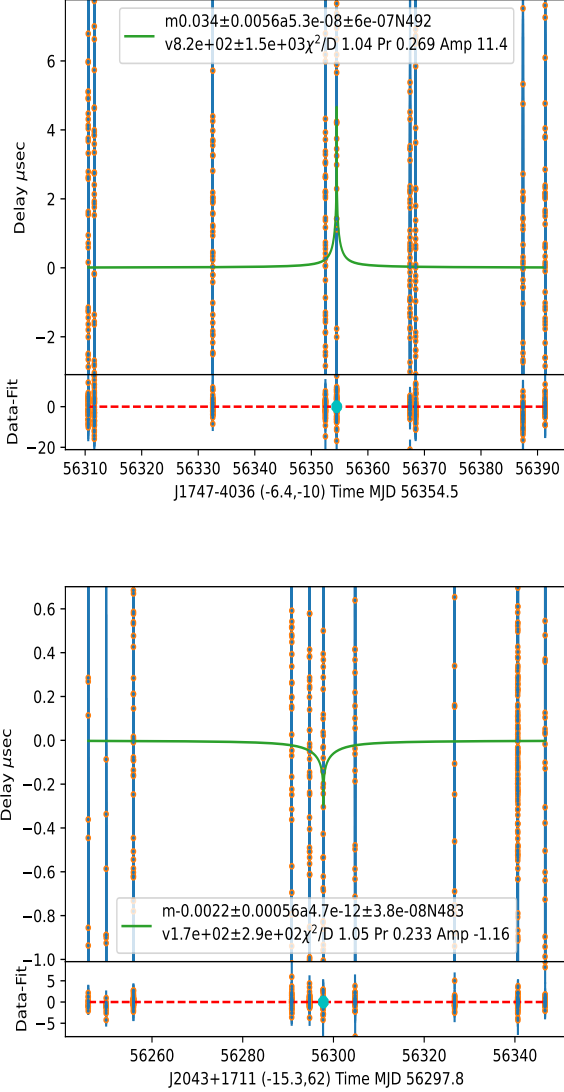


**Figure 12.** The fits for the two candidate events found in the red noise subtracted data.

imposed bounds. The RMS set the scale for the amplitude, the duration set a limit on detectable velocities and the sample spacing and short term noise limited the sensitivity to the impact parameter.

## 11 FUTURE POSSIBILITIES

Classic gravitational lensing [Refsdal \(1964\)](#) provides three observables, the time delay used in this analysis, amplification of the signal used in microlensing and multiple images. It may be possible to add these to the pulsar observables. The recorded energy may show changes correlated with the time delays or one may be able to discern changes in the apparent source size correlated with the delay. Even modest additional input may help reject noise events and better characterize true lensing sources.

## ACKNOWLEDGMENTS

This work would not have been possible without the efforts of the maintainers of the IPTA second data release and the Tempo2 code used to fit the residuals. Jim Rich has been an invaluable aid in understanding the microlensing method of observing dark matter that has many concepts in common with those used here. The author is grateful to an anonymous referee who identified several shortcomings in an earlier version of the manuscript.

## DATA AVAILABILITY

The data underlying this article is from the IPTA second data release [IPTA \(2019\)](#) which is publicly available. Please see their article for details on how to access the data sample. The computer code for this analysis is available from the author. Tempo2 is available from its authors [Edwards \(2006\)](#).

## REFERENCES

- J. Antoniadis *et al.*, “The International Pulsar Timing Array second data release: Search for an isotropic Gravitational Wave Background”, *MNRAS*, **510** 4873-4887 (2022).
- R.T. Edwards, G.B. Hobbs, R.N. Manchester, “tempo2, a new pulsar timing package – II. The timing model and precision estimates”, *MNRAS*, **372**, 1549-1574 (2006).
- B. Goncharov *et al.*, “Identifying and mitigating noise sources in precision pulsar timing data sets”, *MNRAS*, **502**, 478-493 (2021).
- M. Kerr *et al.*, “The Parkes Pulsar Timing Array project: second data release”, *Publications of the Astronomical Society of Australia*, **37**, e020 (2020)
- D.J. Reardon *et al.*, “The Parkes pulsar timing array second data release: Timing analysis”. *MNRAS*, **507**, 2137-2153 (2021).
- T.I. Larchenkova and O.V. Doroshenko, “Pulsars as a Tool for Detection of Dark Matter in the Galaxy” *Astron. Astrophys.* **297**, 607-609 (1995)
- T.I. Larchenkova and S. M. Kopeikin, “Shapiro Effect as a Possible Cause of the Low-Frequency Pulsar Timing Noise in Globular Clusters”, *Astro. Lett.* **32** (1):18-28 (2006)
- T.I. Larchenkova and A.A. Lutovinov (2007), “On the Possibility of Observing the Shapiro Effect for Pulsars in Globular Clusters”, *Astro. Lett.* **33** (7): 455-467 (2007)
- S. Desai and E.O. Kahya (2016), “Galactic one-way Shapiro delay to PSR B1937+21”, *Mod. Phys. Lett. A* **31** (13): 1650083-1 - 1650083-14 (2016).
- Ting-Hang Pei, “The Superluminal Phenomenon of Light Near the Kerr–Newman Black Hole or Super-Gravitational Source”, *Front. Phys.*, Volume 9 - 2021 | <https://doi.org/10.3389/fphy.2021.701619> (2021).
- Tien Hsieh, Da-Shin Lee and Chi-Yong Lin. “Gravitational time delay effects by Kerr and Kerr–Newman black holes in strong field limits”, *Phys. Rev D* **104**. 104013 (2021).
- BBP. Perera *et al.* “The International Pulsar Timing Array: second data release”. *MNRAS*, **490**, 4666-4687 (2019)
- Sjur Refsdal, “The Gravitational Lens Effect”, *MNRAS*, **128** 295-306 (1964).
- Irwin I. Shapiro (1964), “Fourth Test of General Relativity”, *Phys. Rev. Lett.* **13** (26): 789-791 (1964).
- S. Weinberg, “Gravitation and Cosmology”, Wiley & Sons, New York, (1972).
- Irwin I. Shapiro *et al.*, “Fourth Test of General Relativity: Preliminary Results”, *Phys. Rev. Lett.* **20**, 1265-1269 (1968).

L. Wyrzykowski *et al.*, “Gaia Data Release 3 Microlensing Events from All Over the Sky” *Astron. Astrophys.* **abc**, 1-45 (2022). (arXiv:2206.06121)

This paper has been typeset from a T<sub>E</sub>X/L<sup>A</sup>T<sub>E</sub>X file prepared by the author.